Acta Crystallographica Section D
Biological Crystallography
ISSN 0907-4449

On the routine use of soft X-rays in macromolecular crystallography

Manfred S. Weiss,[a]* Tom Sicker,[a] Kristina Djinovic-Carugo[b] and Rolf Hilgenfeld[a]

[a]Institute of Molecular Biotechnology, Department of Structural Biology and Crystallography, PO Box 100813, D-07708 Jena, Germany, and [b]Structural Biology Laboratory, Sincrotrone Trieste in AREA Science Park, 34102 Basovizza (TS), Trieste, Italy

Correspondence e-mail: msweiss@imb-jena.de

Received 29 November 2000
Accepted 21 February 2001

A diffraction data set has been collected from a blood coagulation factor XIII–Ca^{2+} complex crystal at the X-ray diffraction beamline of the ELETTRA synchrotron (Trieste, Italy) at a wavelength of 2.6 Å. The data collection could be carried out using the beamline as is, without making any time-consuming changes to the apparatus. Various data-processing schemes have been employed and it has been observed that local or detector scaling procedures are essential for producing the 'best' anomalous differences.

1. Introduction

Ever since the beginning of the 1990s when soft X-rays were first employed in macromolecular crystallography, interest in the use of long-wavelength X-radiation to address various problems has been continuously growing (for a recent review, see Carpentier *et al.*, 2000). There are several reasons for this. First of all, collection of anomalous diffraction data at the *M* edge of the very heavy elements such as uranium would provide a very large signal for phase determination based on anomalous diffraction intensity differences. For example, $\Delta f''$ of uranium at its M_V edge ($\lambda = 3.5$ Å) can be as large as 110 e (Hendrickson & Ogata, 1997) owing to an intense white line. Experiments on a uranyl derivative of asparaginyl-tRNA synthetase have recently been carried out by Kahn *et al.* (2000). However, owing to various experimental problems such as absorption, low detector sensitivity and large scattering angles, only partial data sets to low resolution could be recorded.

The L_{III} edge of xenon at a wavelength of about 2.6 Å with a $\Delta f''$ of about 11 e (Table 1) offers another important potential application. Xenon derivatization of proteins is often relatively easy and since Xe does not chemically react with the protein it is considered an attractive heavy atom for phasing by isomorphous replacement (Djinovic-Carugo *et al.*, 1998). The *K* edge of Xe at about 0.3 Å is out of reach for most synchrotron sources, although there have been attempts to make use of it (Schiltz *et al.*, 1997).

Other possible applications of soft X-rays in biological crystallography centre around the enhancement of the anomalous signal of sulfur and phosphorus and the use of these elements as markers in macromolecular structure determination (Stuhrmann *et al.*, 1997; Behrens *et al.*, 1998) or the use of the enhanced anomalous sulfur signal in single-wavelength anomalous scattering (SAS) experiments for phase determination (Chayen *et al.*, 2000). A few theoretical values for the anomalous scattering factors of selected elements at various wavelengths are listed in Table 1. Hendrickson & Teeter (1981) demonstrated that the anom-

Table 1
Anomalous scattering factors $\Delta f''$ (e).

The values for $\Delta f''$ are based upon the theoretical approximation developed by Cromer & Liberman (1970). They were retrieved from the internet site of the Biomolecular Structure Center at the University of Washington, Seattle, USA (http://www.bmsc.washington.edu/scatter/AS_periodic.html).

	λ (Å)					
Element	1.0	1.54 (Cu *Kα*)	2.0	2.29 (Cr *Kα*)	2.5	3.0
O	0.01	0.03	0.06	0.07	0.09	0.13
P	0.19	0.43	0.71	0.91	1.05	1.45
S	0.24	0.56	0.90	1.15	1.33	1.82
Cl	0.31	0.70	1.12	1.43	1.66	2.24
Ca	0.59	1.29	2.01	2.53	2.88	3.89
Xe	3.6	7.1	11.1	11.7	10.1	4.3
U	6.9	13.4	19.8	23.1	25.0	33.0

alous signal of sulfur at a wavelength of 1.54 Å provided sufficient phasing power in the structure determination of crambin and recently Dauter *et al.* (1999) proved that carefully measured, complete and highly redundant data at a wavelength of 1.54 Å from a synchrotron source yielded anomalous differences that were of sufficiently high quality to determine the structure of hen egg-white lysozyme. In principle, data from a rotating Cu anode should provide the same information, as demonstrated by Weiss (2001).

In cases of systems that are too large to be amenable to direct phase determination by SAS based on sulfur anomalous differences, the enhanced anomalous signal may still be used to aid in the chain tracing by marking sulfur positions or to distinguish certain ions such as K^+, Ca^{2+} or Cl^- from solvent molecules (See Table 1) or from other ions. A demonstration of this was provided for instance by Einspahr *et al.* (1985), who managed to distinguish Mn^{2+} from Ca^{2+} on the basis of anomalous differences measured at a wavelength of 1.896 Å (Mn *K* edge).

If only small or weakly diffracting crystals are available, it may be advantageous to make use of the fact that the uncorrected intensity of the scattered wave is proportional to the third power of λ. It has already been suggested by Teplyakov *et al.* (1998) that to balance absorption and scattering, the optimal data-collection wavelength for small crystals may be longer than for large crystals. A second practical aspect is that the larger scattering angles make it easier to measure the very low resolution reflections which are otherwise obstructed by the beamstop. One has to keep in mind, however, that the larger scattering angles will simultaneously lower the high-resolution limit of the measurable data.

The various advantages of soft X-rays have also prompted some researchers to explore the possibility of their use in macromolecular crystallography on a laboratory source. Anderson *et al.* (1996) have tried to enhance the anomalous sulfur signal by collecting diffraction data using X-rays from a chromium anode (λ = 2.29 Å at Cr *Kα*) and Kwiatkowski *et al.* (2000) have constructed a three-metal anode of gold, copper and chromium for pseudo-MAD experiments to be carried out in their laboratory.

Our objective was to use the enhanced anomalous signal of calcium at a wavelength as close as possible to the calcium *K* edge (λ = 3.07 Å) to identify weakly occupied calcium sites in blood coagulation factor XIII crystals and to distinguish them from solvent sites. We have tried to collect the data at the X-ray diffraction beamline at the ELETTRA synchrotron (Trieste, Italy) with practically no modification to the beamline setup and we present our experiences in collecting, processing and analysing these data.

2. Materials and methods

Test diffraction images were taken of a crystal of nitrous oxide reductase from *Paracoccus denitrificans* at the X-ray diffraction beamline at the ELETTRA synchrotron (Trieste, Italy). These crystals belong to space group $P2_1$, with unit-cell parameters a = 102.7, b = 105.3, c = 116.6 Å, β = 110.6°.

Crystals of blood coagulation factor XIII were grown as described by Hilgenfeld *et al.* (1990) and by Weiss *et al.* (1998). The protein crystallizes in space group $P2_1$, with one C_2-symmetric homodimer per asymmetric unit. Each chain consists of 731 amino acids and has the chemical composition $C_{3706}H_{5765}N_{1013}O_{1110}S_{28}$ (molecular weight 83 kDa). Of the 28 S atoms per chain, nine occur in cysteine residues, none of which is involved in a disulfide bond, and 19 occur in methionine residues.

A crystal of factor XIII was soaked for 17 h in reservoir solution containing 100 m*M* $CaCl_2$ and afterwards for 1 h in reservoir solution containing 100 mM $CaCl_2$ and 30%(*v*/*v*) glycerol. It was then flash-cooled in a nitrogen stream at 100 K. Diffraction data were recorded at the X-ray diffraction beamline at ELETTRA (Trieste, Italy) at two wavelengths, λ_1 = 2.583 Å and λ_2 = 0.861 Å (= $\lambda_1/3$). Data-collection parameters are given in Table 2. The whole data-collection process including both wavelengths lasted about 30 h.

The data collected at λ_2 = 0.861 Å were integrated and scaled using the programs *DENZO* and *SCALEPACK* (Otwinowski & Minor, 1997). Using the option NO MERGE ORIGINAL INDEX in *SCALEPACK*, scaled but unmerged intensities were written out and the redundancy-independent merging *R* factor $R_{\rm r.i.m.}$ (Weiss & Hilgenfeld, 1997; Diederichs & Karplus, 1997*a*,*b*) as well as the precision-indicating merging *R* factor $R_{\rm p.i.m}$ (Weiss & Hilgenfeld, 1997) were calculated using our own program *RMERGE* (available from http://www.imb-jena.de/www_sbx/projects/sbx_qual.html or from the authors upon request). The data-processing statistics are shown in Table 2. Structure-factor amplitudes were then calculated from the intensities using the method of French and Wilson as implemented in the program *TRUNCATE* (French & Wilson, 1978; Collaborative Computational Project, Number 4, 1994). For the use of this data set as reference data for scaling, it was also processed using *MOSFLM* version 6.01 (Collaborative Computational Project, Number 4, 1994) and *XDS* (Kabsch, 1988).

The data collected at λ_1 = 2.583 Å were integrated and scaled employing seven different schemes: (i) the program *DENZO* (Otwinowski & Minor, 1997) was used for integra-

Table 2
Data-collection and processing parameters.

Values in parentheses refer to the outermost resolution shell.

	Factor XIII (long wavelength)	Factor XIII (reference)
Data collection		
Number of crystals	1	1
Wavelength (Å)	2.583	0.861
Total rotation range (°)	187	188
Rotation range per image (°)	1.0	1.0
Exposure time per image (dose units)	4000–8000	500
Exposure time per image (min)	∼6.5	∼0.5
Total data-collection time (h)	23	5
Detector type	MAR 345	MAR 345
Detector diameter used (mm)	240	300
Crystal-to-detector distance (mm)	90	320
Data processing†		
Unit-cell parameters		
a (Å)	133.25	133.25
b (Å)	70.80	70.79
c (Å)	100.71	100.70
β (°)	105.84	105.87
Resolution limits (Å)	33.2–2.90 (3.00–2.90)	13.8–2.20 (2.28–2.20)
Total No. of reflections	145598	334529
Unique reflections	38491	90332
Redundancy	3.8	3.7
Completeness(%)	95.3 (90.2)	98.1 (97.7)
$I/\sigma(I)$	11.1 (6.2)	15.6 (1.8)
$R_{\rm merge}$‡ (%)	10.4 (16.9)	5.2 (42.2)
$R_{\rm r.i.m.}$§ (%)	12.1 (19.8)	6.1 (49.5)
$R_{\rm p.i.m.}$¶ (%)	6.1 (10.3)	3.1 (25.6)
$R_{\rm anom}$†† (%)	5.9 (10.7)	3.4 (32.9)

† The data-processing parameters presented in this table are based upon the processing scheme *DENZO*/*SCALEPACK*. ‡ $R_{\rm merge} = \sum_{hkl}\sum_i |I_i(hkl) - \overline{I(hkl)}|/\sum_{hkl}\sum_i I_i(hkl)$, where $\sum_{hkl}$ denotes the sum over all reflections and $\sum_i$ the sum over all equivalent and symmetry-related reflections (Stout & Jensen, 1968). § $R_{\rm r.i.m.}$ is the redundancy-independent merging R factor (Weiss & Hilgenfeld, 1997), which is identical to the $R_{\rm meas}$ of Diederichs & Karplus (1997*a*,*b*). $R_{\rm r.i.m.} = \sum_{hkl}(N/N-1)^{1/2}\sum_i |I_i(hkl) - \overline{I(hkl)}|/\sum_{hkl}\sum_i I_i(hkl)$, with N being the number of times a given reflection has been observed. ¶ $R_{\rm p.i.m.}$ is the precision-indicating merging R factor (Weiss & Hilgenfeld, 1997). $R_{\rm p.i.m.} = \sum_{hkl}(1/N-1)^{1/2}\sum_i |I_i(hkl) - \overline{I(hkl)}|/\sum_{hkl}\sum_i I_i(hkl)$. †† $R_{\rm anom} = \sum_{hkl}|I(hkl) - I(\overline{hkl})|/\sum_{hkl}\overline{I(hkl)}$.

tion and the program *SCALEPACK* (Otwinowski & Minor, 1997) for scaling, (ii) and (iii) *DENZO* was combined with the scaling program *SCALA* (Collaborative Computational Project, Number 4, 1994), once employing the reference data set and once without, (iv) and (v) the program *MOSFLM* version 6.01 (Collaborative Computational Project, Number 4, 1994) was used for integration and *SCALA* (Collaborative Computational Project, Number 4, 1994) for scaling, again once with the reference data set and once without, and (vi) and (vii) the program *XDS* (Kabsch, 1988) was used for integration and for scaling in combination with *XSCALE*, again once with and once without the reference data set. The statistics for the various data-processing schemes are given in Table 3.

The scaling model applied by the program *SCALEPACK* (Otwinowski & Minor, 1997) consists of one scale and one isotropic temperature factor per recorded diffraction image. This model is equivalent to the BATCH scaling option in *SCALA* (Collaborative Computational Project, Number 4, 1994). When *SCALA* was used to scale the images, an initial BATCH scaling was performed, which was then followed by an interpolated three-dimensional scaling using the rotation angle and the detector (x, y) coordinates of the recorded spots as the three dimensions (DETECTOR scaling). This DETECTOR scaling procedure is similar to that described by Kabsch, which is also employed in the programs *XDS*/*XSCALE* (Kabsch, 1988). When a reference data set was included, a local scaling procedure was employed to scale the long-wavelength data against the reference data set.

The 1.6 Å structure of the blood coagulation factor XIII–Ca^{2+} complex (unpublished results) was refined against the data collected at λ_2 = 0.861 Å using the program *CNS* (Brunger *et al.*, 1998). After one round of refinement, which included rigid-body refinement, 200 cycles of regular least-squares refinement and 50 cycles of individual temperature-factor refinement, the R factor was 20.8% ($R_{\rm free}$ = 24.5%). The phases calculated from the refined model were used to compute the anomalous difference Fourier maps. The maps were computed using the *CCP*4 program *FFT* (Collaborative Computational Project, Number 4, 1994).

3. Results and discussion

3.1. Data collection

Visual inspection of the images in Fig. 1 shows that even though the signal-to-noise ratio in the X-ray photographs becomes smaller as the wavelength increases, images collected at wavelengths of up to 3.0 Å (close to the limit of the monochromator setup at the X-ray diffraction beamline at the ELETTRA synchrotron) still seem to exhibit a sufficiently high signal-to-noise ratio to yield a reasonable diffraction data set. It is important to mention that the photographs were taken without any changes made to the beamline setup. The only modification was a partial evacuation of the double gas-filled beam-position monitor at the end of the beamline. Other work that has been published recently in this field (for a review, see Carpentier *et al.*, 2000) required extensive changes to the beamline setup such as the insertion of extra mirrors into the beampath or the use of helium chambers *etc.* and is, therefore, not suitable for synchrotron users on a routine basis.

The proof-of-principle that a usable diffraction data set can be obtained under such circumstances at a wavelength of approximately 2.6 Å was achieved using a crystal of factor XIII which had been soaked in 100 m*M* $CaCl_2$ for 17 h. The details of the data-collection setup are given in Table 2. Owing to the reduced intensity of the beam at this long wavelength and the relatively strong absorption effects, rather long exposure times had to be used. Furthermore, on the first images of the data set, evidence for the reflections originating from a third-harmonic wavelength was seen. However, since the physical diffraction limit of the crystal used was about 2.0 Å, only the low-resolution range (∞ to about 5–6 Å) was affected by this problem. During the course of the experiment, these additional reflections vanished, which is indicative of a slight misalignment of the monochromator crystals. In future experiments, this could be employed as a means to suppress the third-harmonic reflections altogether. Within a little less

than 1 d, a total rotation range of 187° was covered, which is sufficient to obtain a full set of anomalous differences for all crystal systems but triclinic ones. As we were not sure about how well this data set could be processed owing to the expected severe absorption errors, we collected a second data set over the same rotation range and in the same crystal orientation at a shorter wavelength (λ_2 = 0.861 Å), which could be used as a reference data set for scaling in a similar fashion to that reported by Anderson *et al.* (1996).

3.2. Data processing

In retrospect, data processing and scaling proceeded without any problems. All seven data-processing schemes yielded reasonable data sets as judged from the statistics given in Table 3. It is noteworthy that the combination *DENZO*/*SCALEPACK* yields considerably worse merging statistics than any of the other schemes. The explanation for this is that the scaling model of *SCALEPACK* is by far the simplest of the ones tried. Only one scale and one temperature factor per image is probably not sufficient to correct for the absorption errors. The detector-scaling models employed in *SCALA* and *XDS*/*XSCALE* are much more elaborate and seem to be necessary in this case.

In terms of signal-to-noise ratio as expressed by $I/\sigma(I)$, the four protocols that involve *SCALA* as scaling program yield values that are higher by a factor of 2 than those obtained from the other protocols. The reason for this is not clear to us, since care was taken to ensure the proper estimation of the standard deviations in all cases. This observation may well be another indication of the need for an elaborate scaling protocol, especially for data collected at wavelengths at which absorption becomes a potential problem.

The data sets are not 100% complete despite a rotation range of 187°. This is a consequence of the blind region, the shadow of the beam stop and of the Cryostream nozzle. Furthermore, in the low-resolution area of the detector, reflections originating from the third-harmonic wavelength overlap with the diffraction pattern of interest. This led to a few overloaded reflections and resulted in the rejection of some low-resolution reflections. Another observation is that the *XDS*/*XSCALE* combination yielded data sets of considerably lower completeness, which is likely to be because of a higher default rejection probability. Furthermore, *XDS* (Kabsch, 1988) was originally developed to process multiwire diffraction data and may not be the best choice for processing images with a relatively large rotation range.

As judged by the merging *R* factors, the four data-processing schemes which involve the *SCALA* scaling program clearly appear to be superior to the other three. Still, the $R_{\rm anom}$ is, even in those cases, in the range of the $R_{\rm p.i.m.}$, which is an indicator for the precision of the averaged measurement (Weiss & Hilgenfeld, 1997; Weiss, 2001). The theoretically expected anomalous signal (about 4.2% on

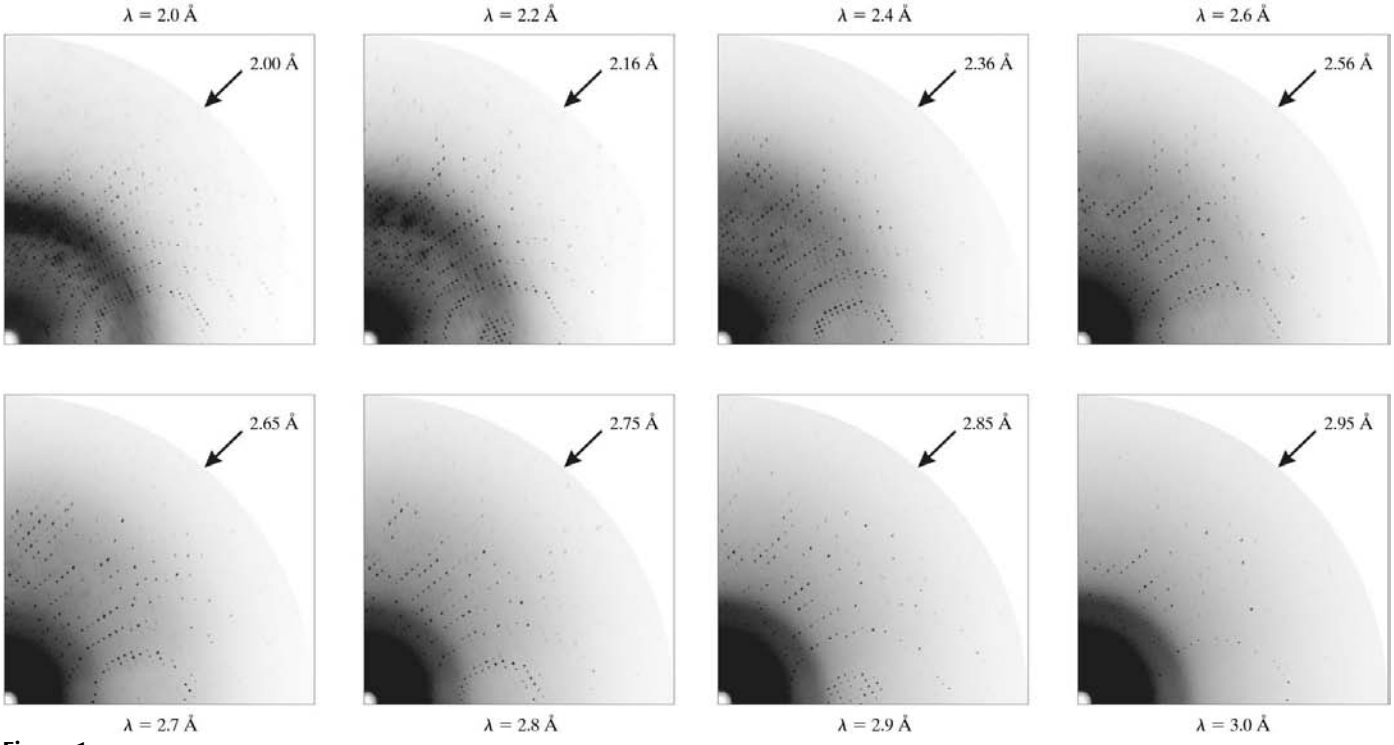

Figure 1
Diffraction images of a crystal of nitrous oxide reductase from *P. denitrificans* taken at wavelengths λ = 2.0, 2.2, 2.4, 2.6 (first row), 2.7, 2.8, 2.9 and 3.0 Å (second row). The best data sets collected from these crystals extend to a resolution of 1.6 Å. The crystal-to-detector distance was 100 mm for the λ = 2.0 Å image and 95 mm for all others and the rotation range was 0.5° in all cases. The exposure time for the various images were 120 s (λ = 2.0 and 2.2 Å images), 180 s (λ = 2.4, 2.6, 2.7, 2.8 Å images and 300 s (λ = 2.9 and 3.0 Å images). In order to make the displayed images comparable, the mean intensity of the images was used to scale them for displaying purposes. The high-resolution limit of all images is indicated by the arrows. Visual inspection shows that a sufficient signal-to-noise ratio can be observed even at a wavelength λ = 3.0 Å.

Table 3
Data-processing statistics: 2.6 Å data set and several processing protocols.

Values in parentheses refer to the outermost resolution shell. n.d., not determined.

	DENZO/*SCALEPACK*	*DENZO*/*SCALA*/*REF*	*DENZO*/*SCALA*	*MOSFLM*/*SCALA*/*REF*	*MOSFLM*/*SCALA*	*XDS*/*XSCALE*/*REF*	*XDS*/*XSCALE*
Resolution limits (Å)	50.0–2.90 (3.00–2.90)	50.0–2.90 (3.00–2.90)	50.0–2.90 (3.00–2.90)	50.0–2.90 (3.00–2.90)	50.0–2.90 (3.00–2.90)	50.0–2.90 (3.00–2.90)	50.0–2.90 (3.00–2.90)
Total No. of reflections	145598	137876	137614	146738	146697	130183	130267
Unique reflections	38491	38101	38101	38281	38290	36440	36458
Redundancy	3.8	3.6	3.6	3.8	3.8	3.6	3.6
Completeness (%)	95.3 (90.2)	94.8 (92.8)	94.8 (92.8)	95.1 (90.4)	95.1 (90.6)	90.2 (85.2)	90.2 (85.3)
$I/\sigma(I)$	11.1 (6.2)	22.6 (13.2)	22.2 (13.2)	23.5 (10.2)	26.3 (10.8)	11.8 (5.4)	11.8 (5.4)
$R_{\rm merge}$ (%)	10.4 (16.9)	5.8 (10.6)	5.9 (10.9)	7.0 (16.5)	6.2 (15.1)	7.6 (17.6)	7.6 (17.5)
$R_{\rm r.i.m.}$ (%)	12.1 (19.8)	6.8 (12.5)	6.9 (12.9)	8.1 (19.3)	7.2 (17.6)	10.1 (22.8)	10.1 (22.7)
$R_{\rm p.i.m.}$ (%)	6.1 (10.3)	3.5 (6.5)	3.6 (6.8)	4.1 (9.8)	3.6 (9.0)	n.d. (n.d.)	n.d. (n.d.)
$R_{\rm anom}$ (%)	5.9 (10.6)	3.8 (7.3)	4.0 (7.5)	4.3 (11.6)	4.1 (10.8)	5.1 (11.1)	5.1 (11.1)

intensities at a wavelength of 2.6 Å) correlates well with the observed anomalous difference as expressed by $R_{\rm anom}$. Therefore, it may be possible to solve the calcium and sulfur substructure of factor XIII based on these anomalous differences and to calculate phases using the SAS approach. Studies along that line are currently under way. However, the anomalous difference Patterson synthesis does not show the expected peaks for the calcium ions, which is likely to be because of the high number of anomalously scattering atoms (two Ca^{2+} ions and 56 S atoms in the aymmetric unit). This observation also means that even the best data set presented in this paper may still contain too much error in the anomalous differences and that even more precisely measured and/or processed diffraction data are necessary. Similarly, smaller systems which exhibit a stronger anomalous signal may be amenable to the SAS approach based on the S atoms in the structure, provided that the anomalous signal can be sufficiently enhanced by collecting data at longer wavelengths so that it is in the range of or smaller than the measurement and averaging error.

3.3. Anomalous difference Fourier maps

In order to assess the quality or the accuracy of the anomalous differences obtained by the various data-processing schemes, anomalous difference Fourier electron-density maps were calculated. As an example, the Fourier summation using the anomalous differences resulting from the processing and scaling scheme *DENZO*/*SCALA*/*REF* is presented in Fig. 2. Since all the electron-density maps look qualitatively similar, five map parameters were used as a quality indicator for the anomalous differences obtained by the seven data-processing and scaling protocols.

(i) The height of the highest peak in the map in units of electron-density map standard deviations: the higher the highest peak was, the better the anomalous differences were presumed to be, since the phase set employed for the calculation of the map was the same in all cases.

(ii) The depth of the minimum of the map in units of standard deviations was considered to be a measure of the noise in the map: the shallower the minimum, the better the anomalous differences.

(iii) The quotient of the maximum electron density and the minimum electron density $\rho_{\rm max}/|\rho_{\rm min}|$: the higher the number, the better the anomalous differences.

(iv) The peak height of the highest spurious peak in the map as another measure of the noise in the map.

(v) The ranking of this peak among all peaks in the map: the higher this peak was and the further up the list of the top peaks it appeared, the worse were the anomalous differences presumed to be.

The results of this analysis are shown in Table 4.

The results of the ranking employing the various criteria are relatively coherent. The largest values for $\rho_{\rm max}/|\rho_{\rm min}|$ were obtained in the four cases that employ *SCALA* as the scaling program. To our surprise, the use of a reference data set improved that situation a little when *DENZO* was used as the integration program and worsened the situation slightly when *MOSFLM* was used to integrate the data. However, the differences are small and probably of no significance. The performance of *XDS*/*XSCALE* and *XDS*/*XSCALE*/*REF* was considerably worse and again the reference data set did not make much of a difference. Trailing behind is the scheme *DENZO*/*SCALEPACK*, which we attribute to the simple scaling model employed, which clearly seems to be insufficient. This could also be deduced from the merging statistics.

With respect to the highest peak in the anomalous difference Fourier map, exactly the same situation is observed, except that *XDS*/*XSCALE* seems to be slightly better than *XDS*/*XSCALE*/*REF*, but again the differences are unlikely to be of any significance.

If we look at the highest peak in the anomalous difference Fourier map that could not be assigned to any known or potential calcium, sulfur or chloride position, the situation is again very similar, except that the differences between the six better protocols have become somewhat smaller. This criterion and the depth of the minimum of the map in units of standard deviations yield surprisingly similar numbers for the noise level in the map.

In the four protocols that involve *SCALA* as the scaling program, the highest spurious peak in the anomalous difference Fourier map occurs much further down in the peak list than in the remaining three protocols, again suggesting that

Table 4
Parameters of the anomalous difference Fourier maps based on Δ_{ano} values from the seven different data-processing schemes.

	DENZO/ SCALEPACK	*DENZO/ SCALA/ REF*	*DENZO/ SCALA*	*MOSFLM/ SCALA/ REF*	*MOSFLM/ SCALA*	*XDS/ XSCALE/ REF*	*XDS/ XSCALE*
$\rho_{max}/\sigma(\rho)$	9.8	15.2	14.1	12.0	12.2	10.5	10.8
$\rho_{min}/\sigma(\rho)$	−6.3	−5.2	−5.2	−5.3	−4.9	−5.0	−5.0
$\rho_{max}/\lvert\rho_{min}\rvert$	1.6	2.9	2.7	2.3	2.5	2.1	2.1
$\rho_{max}/\sigma(\rho)$†	6.6	4.9	5.0	4.7	5.3	5.2	5.6
Peak number‡	20	41	41	37	34	27	24
Total rank§	7	1	2	4	3	5	6

† The values in this row denote the peak height of the highest spurious peak in the anomalous difference Fourier map. ‡ These numbers denote the rank of the highest spurious peak in the complete peak list. § The total rank of the various data-collection schemes is calculated based upon their performance concerning the five parameters listed. For each criterion, an individual rank was determined for each of the seven processing schemes; the five individual rank numbers were then summed and the total rank was determined based on the total sum.

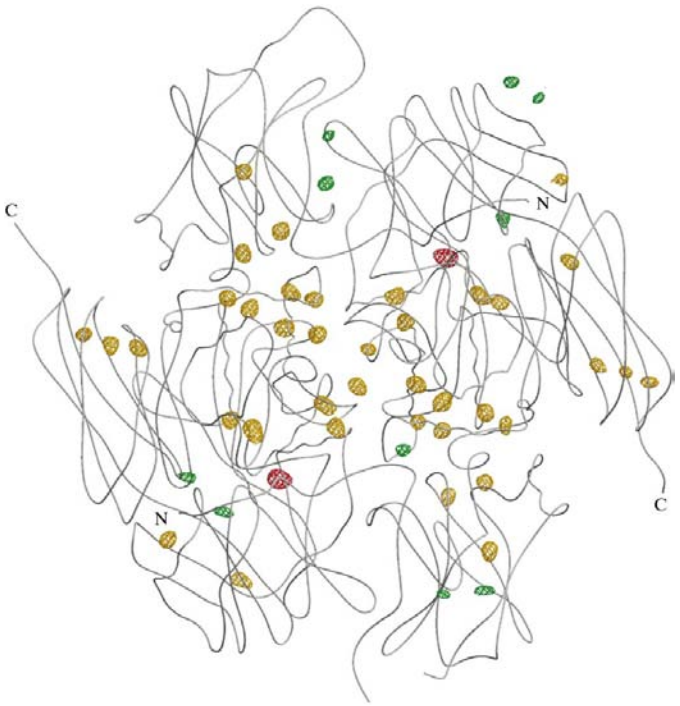

Figure 2
Anomalous difference Fourier summation based on ΔF values obtained from the processing scheme *DENZO*/*SCALA*/*REF*. The top 50 peaks of this map (peak heights 15.2–4.5σ) are displayed at a contour level of 3.0σ and are superimposed on a schematic representation of the factor XIII dimer. The peaks in red denote the known calcium positions, those in yellow sulfur positions and those in green are unassigned or spurious peaks. Of the 56 S atoms in the factor XIII dimer, 38 were found among this list, 14 more appeared with peak heights ranging from 4.5 to 3.0σ (these are not displayed) and the four remaining S atoms exhibit a high mobility (Met512 and Met731 in both chains *A* and *B*) and do not at all appear in the list of peaks. The figure was produced using the program *BOBSCRIPT* (Esnouf, 1997).

the four protocols involving *SCALA* are clearly superior to the other three.

4. Conclusions

We have shown that the collection of diffraction data at long wavelengths is feasible on a routine basis at least up to a wavelength of λ = 2.6 Å. These data can yield valuable information about the positions of anomalously scattering light elements such as P, S, Cl, K, Ca *etc*. in the structure and can potentially be employed for the determination of phases as well.

For processing these data, it appears to be absolutely necessary to employ a suitable scaling scheme in order to correct for the severe absorption effects at those wavelengths, such as the one used in *SCALA*. The detector scaling procedure of *SCALA* seems to be necessary to obtain the 'best' anomalous differences and it seems to be sufficiently elaborate to make the collection of a reference data set at a shorter wavelength unnecessary.

We would like to thank Dr Gottfried J. Palm for his help in collecting the factor XIII data. Recombinant factor XIII (α-chain dimer) was kindly supplied by Dr Hubert J. Metzner (Aventis Behring, Marburg, Germany). This work was carried out within the European Bio-Crystallogenesis Initiative and was supported by the European Commission (Grant No. BIO4-CT98-0086). RH thanks the Fonds der Chemischen Industrie for support.

References

Anderson, D. H., Weiss, M. S. & Eisenberg, D. (1996). *Acta Cryst.* D**52**, 469–480.
Behrens, W., Otto, H., Stuhrmann, H. B. & Heyn, M. P. (1998). *Biophys. J.* **75**, 255–263.
Brunger, A. T., Adams, P. D., Clore, G. M., DeLano, W. L., Gros, P., Grosse-Kunstleve, R. W., Jiang, J.-S., Kuszewski, J., Nilges, M., Pannu, N. S., Read, R. J., Rice, L. M., Simonson, T. & Warren, G. L. (1998). *Acta Cryst.* D**54**, 905–921.
Carpentier, P., Berthet-Colominas, C., Capitan, M., Chesne, M.-L., Fanchon, E., Lequien, S., Stuhrmann, H., Thiaudière, D., Vicat, J., Zielinski, P. & Kahn, R. (2000). *Cell. Mol. Biol.* **46**, 915–935.
Chayen, N. E., Cianci, M., Olczak, A., Raftery, J., Rizkallah, P. J., Zagalsky, P. F. & Helliwell, J. R. (2000). *Acta Cryst.* D**56**, 1064–1066.
Collaborative Computational Project, Number 4 (1994). *Acta Cryst.* D**50**, 760–763.
Cromer, D. T. & Liberman, D. A. (1970). *J. Chem. Phys.* **53**, 1891–1898.
Dauter, Z., Dauter, M., de La Fortelle, E., Bricogne, G. & Sheldrick, G. M. (1999). *J. Mol. Biol.* **289**, 83–92.

Diederichs, K. & Karplus, P. A. (1997*a*). *Nature Struct. Biol.* **4**, 269–275.
Diederichs, K. & Karplus, P. A. (1997*b*). *Nature Struct. Biol.* **4**, 592.
Djinovic-Carugo, K., Everitt, P. & Tucker, P. A. (1998). *J. Appl. Cryst.* **31**, 812–814 (1998).
Einspahr, H., Suguna, K., Suddath, F. L., Ellis, G., Helliwell, J. R. & Papiz, M. Z. (1985). *Acta Cryst.* B**41**, 336–341.
Esnouf, R. M. (1997). *J. Mol. Graph.* **15**, 132–134.
French, G. S. & Wilson, K. S. (1978). *Acta Cryst.* A**34**, 517–525.
Hendrickson, W. A. & Ogata, C. M. (1997). *Methods Enzymol.* **276**, 494–523.
Hendrickson, W. A. & Teeter, M. M. (1981). *Nature (London)*, **290**, 107–113.
Hilgenfeld, R., Liesum, A., Storm, R., Metzner, H. J. & Karges, H. E. (1990). *FEBS Lett.* **265**, 110–112.
Kabsch, W. (1988). *J. Appl. Cryst.* **21**, 916–924.
Kahn, R., Carpentier, P., Berthet-Colominas, C., Capitan, M., Chesne, M.-L., Fanchon, E., Lequien, S., Thiaudière, D., Vicat, J., Zielinski, P. & Stuhrmann, H. (2000). *J. Synchrotron Rad.* **7**, 131–138.
Kwiatkowski, W., Noel, J. P. & Choe, S. (2000). *J. Appl. Cryst.* **33**, 876–881.
Otwinowski, Z. & Minor, W. (1997). *Methods Enzymol.* **276**, 307–326.
Schiltz, M., Kvick, Å., Svensson, O. S., Shepard, W., de La Fortelle, E., Prangé, T., Kahn, R., Bricogne, G. & Fourme, R. (1997). *J. Synchrotron Rad.* **4**, 287–297.
Stout, G. H. & Jensen, L. H. (1968). *X-ray Structure Determination. A Practical Guide*. London: Macmillan.
Stuhrmann, S., Bartels, K. S., Braunwarth, W., Doose, R., Dauvergne, F., Gabriel, A., Knöchel, A., Marmotti, M., Stuhrmann, H. B., Trame, C. & Lehmann, M. S. (1997). *J. Synchrotron Rad.* **4**, 298–310.
Teplyakov, A., Oliva, G. & Polikarpov, I. (1998). *Acta Cryst.* D**54**, 610–614.
Weiss, M. S. (2001). *J. Appl. Cryst.* **34**, 130–135.
Weiss, M. S. & Hilgenfeld, R. (1997). *J. Appl. Cryst.* **30**, 203–205.
Weiss, M. S., Metzner, H. J. & Hilgenfeld, R. (1998). *FEBS Lett.* **423**, 291–296.